NASA TECHNICAL MEMORANDUM

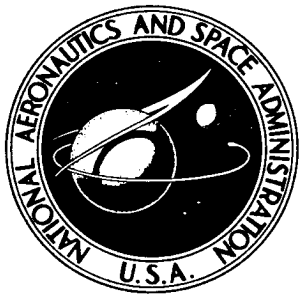

UB
NASA TM X-1612

BASE PRESSURE MEASUREMENTS ON THE XB-70 AIRPLANE AT MACH NUMBERS FROM 0.4 TO 3.0

by Edwin J. Saltzman, Sheryll A. Goecke, and Chris Pembo

Flight Research Center
Edwards, Calif.

NATIONAL AERONAUTICS AND SPACE ADMINISTRATION • WASHINGTON, D. C. • SEPTEMBER 1968

NASA TM X-1612

BASE PRESSURE MEASUREMENTS ON THE XB-70 AIRPLANE AT MACH NUMBERS FROM 0.4 TO 3.0

By Edwin J. Saltzman, Sheryll A. Goecke, and Chris Pembo

Flight Research Center
Edwards, Calif.

NATIONAL AERONAUTICS AND SPACE ADMINISTRATION

BASE PRESSURE MEASUREMENTS ON THE XB-70 AIRPLANE AT MACH NUMBERS FROM 0.4 TO 3.0*

By Edwin J. Saltzman, Sheryll A. Goecke, and Chris Pembo
Flight Research Center

SUMMARY

Full-scale flight base pressure coefficients obtained from the XB-70 propulsion package are compared with predicted values based on a combination of cold jet flow wind-tunnel models and data from a two-engine side-by-side jet, full-scale aircraft. At cruise Mach numbers the base pressures on the full-scale aircraft were higher than predicted, resulting in a favorable increment of about 2 percent in terms of lift-drag ratio.

At low supersonic speeds near a Mach number of 1.2, the negative base pressure coefficients were about three times larger than predicted, which would result in a significant lift-drag-ratio decrement.

The investigation showed that the net calculated effect of underestimating the base drag at low supersonic climbout speeds, even though overestimating the base drag at cruise, can seriously reduce the range potential of the aircraft, depending on several operational factors that can influence transonic excess thrust. The trend of this range decrement (with respect to the transonic excess thrust) emphasizes the need for a base drag prediction based on models with a higher degree of similitude throughout the transonic and supersonic speed range.

INTRODUCTION

It is well known that base drag can be a relatively large part of the total drag of multiengine aircraft at low supersonic speeds. For some large supersonic aircraft the base component of drag can become a serious performance and operational problem. This problem occurs when the flight trajectories for maximum transonic excess thrust become incompatible with operational restrictions that may be common to supersonic transport aircraft. Unfortunately, the incompatibility is most adverse at the Mach numbers at which base drag coefficients are the highest. Therefore, base drag becomes of interest operationally in addition to its effects on efficiency.

Many investigators have studied afterbody and base aerodynamics to determine which fluid dynamic parameters are most important, what is the most realistic analytical flow model, and how base drag can be predicted and reduced. Theoretical and

*Title, unclassified.

semiempirical methods have been developed to predict base pressures for design purposes (refs. 1 to 10), and the adequacy of these methods continues to be assessed primarily by comparison with wind-tunnel results.

Such wind-tunnel-model studies have been conducted for a variety of configurations with and without a simulated jet exhaust. The adequacy of these model results must also be evaluated lest the analytical flow models, theoretical methods, and the prediction techniques, per se, be based on unrealistic criteria.

Where possible, it is desirable to evaluate prediction techniques, usually a combination of theory, wind-tunnel-model results, and prediction experience, by comparison with full-scale flight data. Such flight data have been relatively limited; however, base pressures have been measured recently on the XB-70 airplane. It is believed that these data will be of interest to the designer in that they represent the Mach number range, the jet pressure ratios, and a size of vehicle that are applicable to afterbody flow problems that may be encountered on future supersonic and hypersonic transports.

This paper presents full-scale flight base pressure data from the XB-70-2 airplane obtained during the expansion of the performance envelope to the design Mach number. The base pressure coefficients presented were derived from pressures sensed at 11 base taps on the right half of the six-engine propulsion package. Base pressure coefficients are presented for Mach numbers between 0.4 and 3.0 and for forebody Reynolds numbers from 100 million to 600 million. These data are compared with wind-tunnel model data and with semiempirical estimates.

SYMBOLS

$C_{p,b}$	base pressure coefficient, $\frac{p_b - p}{q}$
$\Delta C_{p,b}$	estimated error in measured base pressure coefficient
D_b	thickness (height) of projected base
D_j	diameter of the jet at jet exit station
L/D	lift-to-drag ratio
$\Delta\frac{L}{D}$	lift-drag-ratio increment
l	length
M	free-stream Mach number
M_j	Mach number of jet exhaust at jet exit station
p	free-stream static pressure
p_b	base pressure

$p_{t,j}$ total pressure at jet exit station

N_{Re} free-stream Reynolds number, $\frac{\rho V l}{\mu}$

q free-stream dynamic pressure, $0.7M^2p$

V true airspeed

w width of propulsion package

α angle of attack

β_l boattail angle of lower surface

β_s boattail angle of side surface

β_u boattail angle of upper surface

μ absolute viscosity

ρ air density

Subscripts:

max maximum

min minimum

Averaged values of various quantities are denoted by a bar, for example, $\overline{M}$.

AIRPLANE

The XB-70 airplane (fig. 1) was originally designed as a weapons system with long-range supersonic-cruise capabilities. The airplane has a design gross weight in excess of 500,000 pounds (227,000 kilograms), design cruising speed of Mach 3.0 at altitudes of 70,000 feet to 80,000 feet (21,300 meters to 24,400 meters), and intercontinental ranging capability. It has a thin, low-aspect-ratio, 65.6°-leading-edge delta wing with folding wing tips, twin vertical stabilizers with rudders, elevon surfaces for the primary pitch and roll control, and a movable canard geared to the elevator action of the elevons to augment rotation during takeoff.

Propulsion is provided by six YJ93-GE-3 engines; each engine has about 28,000 pounds (124,550 newtons) of thrust at sea level, and the compressor has a capacity of 264 pounds (120 kilograms) of air per second. Each engine has an 11-stage axial-flow compressor, an annular combustion section, a two-stage turbine, and a variable-area convergent-divergent exhaust nozzle.

The six engines are mounted side by side in the rear of the fuselage in a single integrated package under the center section of the wing. The propulsion package is

divided into twin, two-dimensional, vertical ramp, mixed-compression inlets incorporating variable ramp positions and throat areas for optimum operation throughout the Mach number range.

The left- and right-hand air-intake ducts are each equipped with inlet-air bypass doors on top of each duct just forward and inboard of the leading edge of the vertical fins (fig. 2). These doors are used in conjunction with the controlled width of the two-dimensional throats to control the position of the normal shock in each of the ducts, and to match engine airflow requirements. Maximum bypass-door setting takes place at a Mach number of 2; zero or near zero bypass setting takes place at a Mach number of 3. The positions of the throat and the bypass doors are determined automatically by the air induction control system, but there is a manual backup system.

The XB-70 incorporates engine secondary airflow and base bleed. Air is bled through perforated panels at the ramp region of the air-inlet ducts and distributed to the base through ducts leading to each of the engine compartments (fig. 3).

General physical characteristics of the airplane are presented in table I, and more detailed characteristics are available in reference 11. Pertinent base and engine dimensions are given in table II.

The base region of the XB-70 is somewhat unusual in that the upper and lower boattail surfaces terminate at different longitudinal stations, causing the engine nozzles to "overhang" the lower boattail (fig. 4). The base region of the XB-70 has no aft-facing bulkhead type of surface; the most aft surface of this type is the engine rear firewall at fuselage station 2102 (5339) which is about 15 feet (4.6 meters) forward of the engine jet exit plane (fig. 5).

INSTRUMENTATION

The location of each orifice used to obtain base pressures is shown in figure 6. These orifices were connected to differential-pressure transducers of a type that utilizes the linear-variable-differential transformer principle. These differential transducers were mounted near the firewall and referenced to a plenum chamber which was vented to the aft set of the nose-boom static-pressure orifices. The reference pressure, i.e., the plenum pressure, was measured by a high-resolution absolute-pressure transducer which was kept in a carefully controlled temperature environment.

The differential transducers were connected by six-conductor shielded cables to the instrumentation package which contains a circuitry card. (A symmetry sensing card is provided for each transducer.) The transducer-conductor-circuitry card system is designed to minimize the effects of temperature. The output from the card module is then routed to the digital recording system, a pulse code modulation (PCM) tape recorder. All records were synchronized by a time-code generator.

Free-stream static (subject to position effects) and impact pressures were sensed by absolute-pressure transducers which were contained in a carefully controlled environment These static and impact pressures were sensed from nose-boom stations 71 inches (180 centimeters) and 77.5 inches (197 centimeters), respectively, ahead of the boom-nose intersection. Nose-boom static pressure has been calibrated in flight

by a combination of several methods, among them radiosonde-radar, radar velocity including winds, pacer, and radiosonde-stagnation temperature. In addition, wind-tunnel calibrations of the boom and forebody position error have been made from $M \approx 0.3$ to $M = 3.0$.

ERROR AND RELIABILITY

The estimated magnitudes of random and bias errors affecting the averaged base pressure coefficients are:

M	Random	Bias
	$\Delta C_{p,b}$, root mean square	$\Delta C_{p,b}$, limit
1.2	±0.013	+ or - 0.012
2.0	±0.013	+ or - 0.011
2.8	±0.017	+ or - 0.018

These values of estimated error are based on experience with the data system, the physical characteristics of the system, and examination of the types of data irregularities that did or did not occur.

Theoretically, the largest source of random error should be the individual differential-pressure transducers. Examination of the results from the 11 base pressure transducers and other similar transducers sensing boattail pressures indicates that this source of random error was about 0.01 in pressure coefficient. When base pressure coefficients are averaged and then faired with respect to Mach number, this source of random error is virtually eliminated.

The bias-error estimates are labeled as a limit rather than as a root mean square because these errors are so few that they occur additively and reach a limit value relatively often as compared to a normal Gaussian distribution, where many error sources are involved. However, the bias errors may also have unknown but opposite signs, and because no single bias source is of a dominant magnitude, the net bias error may also vary from negligible values to one-half the limit values shown in the table.

The problem of pressure lag was studied by comparing results for stabilized flight with accelerating or decelerating flight. It was found that lag effects would be present only for the Mach number increment between about 0.95 to 1.05. Such lag effects, however, would not influence the conclusions of this report.

TEST CONDITIONS

Base pressure data were obtained during performance-envelope-expansion flights over a Mach number range from about 0.4 to near 3.0. Pressure altitude ranged from about 3300 feet (1000 meters) to 72,000 feet (22,000 meters). Unit Reynolds number varied from about 1.05×10^6 to 3.72×10^6 per foot (3.44×10^6 to 12.20×10^6 per meter), thus, even the lower base station, with the shortest forebody, represented

total Reynolds numbers of 100 million to 370 million. A portion of the upper base station experienced flow originating at the aircraft nose, which represents Reynolds numbers up to 600 million. Because of these relatively high Reynolds numbers, the flow approaching the base was always turbulent. Angle of attack varied from about 2.0° to 9.5°, and angle of sideslip varied from 3.0° to -2.4°.

Quantitative definitions of the relationship of bypass mass flow or base bleed with base pressure coefficient cannot be made. However, the data obtained in this study do show that maximum bypass-door opening causes an inflection in the base pressure coefficient–Mach number curve.

At $M \approx 1.2$, where base drag is greatest, base bleed to engines 2, 3, 4, and 5 was between 3 percent and 6 percent of the total exhaust flow from each of the engines. Engines 1 and 6 experienced between 1.5 percent and 3 percent base bleed because their engine bays had only one bleed tube instead of two.

The engines were operating mainly in the maximum afterburner condition for these tests. Other conditions, such as exhaust jet Mach number and jet pressure ratio, that affect the data presented are shown in pertinent figures.

RESULTS AND DISCUSSION

Presentation of Flight Results

Figure 7 shows the variation of base pressure coefficient $C_{p,b}$ with free-stream Mach number M for each of the 11 base-tap locations. These data show that the pressure over the base region is uniform except at the lowest Mach number shown. Because of the great degree of uniformity exhibited by the data in figure 7 and because these data are typical of the great mass of XB-70 base pressure results, the base pressure coefficients shown in subsequent figures are the average of the values from the 11 base taps for a given flight condition.

Figure 8 shows the averaged base pressure coefficients $\overline{C}_{p,b}$ as a function of free-stream Mach number. Several other parameters that affect base pressure are included. Wind-tunnel-model results in references 1 and 3 showed that for turbulent flow conditions, angle of attack and Reynolds number have relatively little influence on base pressure. Full-scale flight results from reference 12 were also found to be relatively insensitive to these variables. Therefore, the flight data presented are plotted without regard to angle of attack or Reynolds number.

Most of the supersonic and high subsonic data in figure 8 represent steady-state conditions; i.e., Mach number and altitude were held constant for periods from 2 minutes to 20 minutes. Included with these data are results from tests at relatively transient flight conditions, particularly in the low supersonic speed range. The relative consistency of the results from flight to flight, in spite of the transient conditions experienced for part of the data, indicates that the pressure-measuring system did not have enough lag to significantly affect the base pressure coefficients, with the exception noted in the ERROR AND RELIABILITY section.

The base pressure-coefficient results in figure 8 display the usual sensitivity of base pressure to Mach number throughout the transonic Mach number range. At Mach numbers above 1.2, the negative base pressure coefficient decays as the usual inverse function of Mach number squared. In this instance, the expression

$$C_{p,b} = \frac{1}{2}\left(-\frac{1}{M^2} + 0.15\right)$$

provides a close approximation of base pressure coefficient over most of the supersonic range.

The slight inflection in the pressure-coefficient data between $M \approx 2.0$ and 2.5 correlates with increased bypass-door deflections (increased bypass area), which are scheduled to maximum area when $M \approx 2.0$. The bypass mass flow is not known well enough, however, to quantitatively define its relationship to base pressure coefficient.

A favorable characteristic of the trend in base pressure coefficient with Mach number for this aircraft is the crossover at $M \approx 2.5$ to positive values. At cruise Mach numbers application of the resulting coefficients over the net base area would result in approximately 600 pounds to 700 pounds (2670 newtons to 3110 newtons) thrust or between 1 percent and 1.5 percent of the cruise drag of the airplane. The resulting base drag is about 2100 pounds (9340 newtons) less than predicted.

The averaged jet total-pressure ratio $\frac{\bar{p}_{t,j}}{p}$ is expected to follow a steadily increasing value with Mach number as shown in figure 8. The trend and level of the data of this study agree with the anticipated schedule of jet total-pressure ratio with Mach number presented in reference 13, which will be typical of large supersonic-cruise aircraft.

The ratio of averaged jet exhaust to base diameter $\frac{\bar{D}_j}{D_b}$ is nearly constant at values corresponding to full afterburner for Mach numbers above approximately 1.8, thus the ratios of nozzle throat to exhaust area tend to be constant and the calculated jet Mach numbers $\bar{M}_j$ are relatively constant at the higher flight velocities for a given flight.

The jet Mach number for flight A is significantly higher than for the other flights. This does not seem to have influenced base pressure, however. Thus, jet Mach number remains secondary in importance to free-stream Mach number, insofar as base pressure is concerned, even when six jets are positioned side by side.

Comparison of Flight Results With Model Data and Semiempirical Estimates for No Jet Flow

It is acknowledged that jet effects should be an important influence on base pressure; therefore, the most meaningful comparisons with wind-tunnel-model results should involve simulated jet flow from the model. Nevertheless, it is also of interest to compare the power-on base pressure characteristics of the somewhat flattened XB-70 afterbody with two-dimensional and body-of-revolution results for models with no jet flow. Thus, the relative severity of base drag of a large jet aircraft can be established with reference to the well-documented base drag of more fundamental shapes.

The average base pressure coefficients from figure 8 are presented in figure 9 as a faired curve, and compared with some no-jet-flow two-dimensional and body-of-revolution data without boattail from references 2 and 3. In addition to the wind-tunnel model data, semiempirical estimates from reference 1 are included, as well as the aforementioned pressure-coefficient decay function, $C_{p,b} = \frac{1}{2}\left(-\frac{1}{M^2} + 0.15\right)$, and the limit value for a vacuum, $C_{p,b} = -\frac{1}{0.7M^2}$.

An obvious, and expected, conclusion from the comparisons shown in figure 9 would be that prediction techniques for side-by-side multiengine-aircraft base pressures must be based on model data with a greater degree of similitude. The comparison also suggests that more realistic model geometry would not be enough and that jet-flow simulation is also required, in that the data for two-dimensional and body-of-revolution shapes, representing afterbody shapes which "bracket" the flattened XB-70 afterbody are both displaced far from the flight power-on results at cruise Mach numbers.

More evidence of the need for additional similarity factors, beyond geometrical considerations, is presented in figure 10 in which wind-tunnel-model results without jet flow are shown for configurations with afterbodies flattened somewhat like that of the XB-70 aircraft. The data from references 13 and 14 are for afterbodies with no boattail. Somewhat greater geometric realism was achieved with the model from reference 15 on which 6° to 7° of boattail and engine-nozzle overhang were included. [1]

The increased geometric realism achieved through boattailing and extending the nozzles had very little effect at $M \approx 3$, although considerable effect may have been experienced had the tests of reference 15 extended to lower supersonic and transonic speeds. Considering the data available for flattened bodies, it is apparent that all of the power-off model results have grossly higher negative base pressure coefficients than experienced by the XB-70 airplane in flight. Thus, it is again apparent, as has been recognized for the last decade, that the prediction of base drag must be based on model studies that include some degree of propulsive jet flow and base-bleed simulation in addition to a practical degree of geometric similarity.

Comparison of Flight Results With Model Data for Simulated Primary Jet Flow

Many studies of jet effects on base pressure have been made. The studies of references 13 to 17, which pertain to side-by-side jet installations for cold-air flow, will be considered in this paper. XB-70 in-flight base pressure coefficients are compared with some of these model data in figure 11. The results from reference 13 are shown for the jet total-pressure-ratio schedule previously included in figure 8 for Mach numbers from approximately 1.6 to 3.0. The corresponding jet-off data are also included. Jet-on and jet-off data from reference 14 are also shown for a somewhat similar model for subsonic and transonic velocities. The results from reference 14 are shown for two different jet Mach numbers that bracket the jet Mach number of the XB-70 for some flights in the subsonic and transonic region.

[1]For the model of reference 15, the nozzles extended aft of the entire base, whereas for the XB-70 the nozzles extend aft of the lower afterbody termination only, as shown in figures 4 and 5.

Results from the boattailed model (ref. 15) are included in figure 11. These data, representing more realistic model geometry, indicate a significant reduction in negative base pressure coefficient with jet flow. Unfortunately, results for jet effects are not available at lower Mach numbers with this model.

Assessment of the model data shown in figure 11 in relation to the XB-70 flight results suggests that even the inclusion of the side-by-side cold-air jets, in addition to a flattened afterbody with boattail and nozzle overhang, results in large simulation deficiencies. In fact, through much of the supersonic speed range, the flattened models, with jet on, have base pressure coefficient levels about half way between the limit values and the XB-70 flight values, which is about the same as the model results for no jet flow. It is apparent that temperature effects, base bleed, the ratio of jet to base diameter, and perhaps other as yet undefined variables must also be accounted for in order to achieve reliable simulation.

Comparisons of Flight Results With Predictions

Base pressure coefficients. – Although the comparisons shown in figure 11 reveal rather large discrepancies between all of the model data and the XB-70 flight results, it is apparent that the model data from reference 15 were the best available for prediction purposes at or near cruise speeds. This was probably the result of the more realistic boundary-layer-to-base scaling, the higher ratios of jet to base diameter, and the greater model geometric, or configuration, similarity. No transonic or low supersonic results were available from this model, however, so the designers were faced with the possibility of using results from less-detailed models, such as those of references 13 and 14, for prediction purposes at these speeds. Another possibility was to utilize flight data from an unmanned full-scale aircraft, the X-10, which had a side-by-side two-engine propulsion package. The designers chose to use the two-engine full-scale flight data for prediction purposes at low supersonic speeds and the data of reference 15, adjusted for the effects of a "hot" jet, bleed flow, and the partial shroud (partial overhang), for the cruise Mach numbers. The subsonic predictions were based on wind-tunnel models with cold jet flow, adjusted for temperature effects. The resulting predictions of base pressure coefficient, from references 18 and 19, are shown in figure 12 with the XB-70 flight results.

The estimates are adequate at Mach numbers up to about 0.95; however, at low supersonic speeds the negative base pressure coefficients were grossly underestimated, in that the full-scale flight XB-70 values of the negative coefficients were about three times larger than predicted. At the higher Mach numbers ($M \geq 2.5$), where the model with the highest degree of similitude was used, a negative base pressure coefficient was predicted; however, the full-scale airplane experienced a positive coefficient above $M = 2.5$. At $M = 2.8$, the increment in coefficient separating the predicted and measured values was about 0.06.

Lift-drag ratio. – The increment of base pressure coefficient that separates the predicted and measured values is interpreted in terms of lift-drag ratio in figure 13. If the aircraft could accelerate quickly through the transonic region and utilize almost all its fuel at cruise conditions, the transonic L/D decrement would be of little consequence and the favorable L/D increment at higher supersonic speeds could be exploited. The favorable increment at cruise speeds is about 2 percent, which corresponds to an increase in cruise range of approximately 0.9 nautical mile per ton of fuel

(1.84 kilometers per metric ton). Thus, the cruise range would be extended beyond the predicted value by 2 percent, minus a range increment attributable to the extra fuel required to accelerate transonically because of the transonic L/D decrement.

Calculated Range Increment Resulting From Discrepancy in Predicting Base Pressure Coefficients

The relative size of the transonic range decrement compared with the theoretical 2-percent favorable increment at cruise speeds depends on the transonic excess thrust available which is, in turn, for a given aircraft, dependent on several factors. Prominent among these factors would be (1) the relative degree of inlet optimization during the climb, (2) deviations of the atmosphere from standard conditions, and (3) climb-profile restrictions dictated by noise-abatement procedures, sonic-boom overpressure criteria, or specific air-traffic problems. It should be noted that although the designers of the XB-70, an experimental bomber, were concerned with the first and second factors, and undoubtedly others, they were not obliged to consider the ramifications of the third factor.

It is of interest, however, to translate the error in predicting base pressure coefficients (from which fig. 13 was derived) into a potential gain or loss in range. To illustrate the possible effect of errors in base pressure prediction on performance, a calculated range increment in terms of excess thrust will be presented. Transonic excess thrust is used as the independent variable because of its relationship to the operational factors noted in the preceding paragraph, especially item 3.

Before presenting the range increment, it may be helpful to show how the base pressure misprediction was used in the range calculations[1]. The transonic base pressure misprediction was first translated into a drag decrement that, when added algebraically to the predicted transonic excess thrust, results in what is referred to herein as available transonic excess thrust. The relationship of predicted and available transonic excess thrust is shown in figure 14(a).

Because the available transonic excess thrust is lower than predicted, the aircraft will take longer to accelerate through the transonic region. The additional time required to accelerate, caused by mispredicting the base pressure, is shown in figure 14(b). Figure 14(c) shows the corresponding difference in the transonic fuel consumption; the actual fuel consumption, of course, is greater than predicted.

The difference in transonic fuel consumption, caused by the misprediction of base pressure, is then translated into an increment in gross range and presented in figure 14(d). The difference parameters (figs. 14(b), (c), and (d)) are presented as a function of the calculated available transonic excess thrust. Figure 14(d) is also presented as a function of the predicted transonic excess thrust that the designer would believe to be available.

Background information on the variation of fuel-flow rates, thrust, and drag with Mach number and altitude was obtained from reference 20.

---

[1]For the purposes of this discussion and the simplified calculations for figure 14, beneficial or detrimental effects from other factors influencing aerodynamic or propulsive performance efficiency of the aircraft are ignored. In addition, it was assumed that there were no discrepancies in the base pressure predictions between $M = 1.4$ and 2.6.

In considering the balance between transonic excess thrust and range, the favorable increment in L/D at cruise, where base drag was overestimated, would result in a bonus of about 30 nautical miles (56 kilometers) at 30,000 pounds (133,400 newtons) of available excess thrust. If the available excess thrust is decreased by one-half, however, this bonus in range is canceled by the transonic L/D decrement that results from underestimating the base drag at transonic speeds. A further reduction of available excess thrust by one-half will result in a net loss in range of about 100 nautical miles (185 kilometers) and the range loss increases very rapidly with a further decrease in available excess thrust.

Thus, the net calculated effect of underestimating the base drag at climbout speeds, even though overestimating the base drag at cruise, can seriously compromise the range potential of the aircraft. The trend of the range decrement with respect to the excess thrust emphasizes the need for base pressure predictions that are derived from wind-tunnel models having a higher degree of similitude throughout the transonic and supersonic speed range.

Effect of Two Jets Off

During one flight, engines 4 and 6, on the right side of the XB-70 propulsion package, were inoperative (although windmilling) for a sufficient time to permit evaluation of the effect on base pressure over a part of the Mach number range. These data are shown in figure 15 with the data previously shown for all six engines operating. Also shown are model data from reference 21 that represent a vehicle configuration similar to the XB-70; however, jet effects were not simulated on this model. The base region of the model was vented by flow from the model inlets, and it is believed that this was an important factor in causing low negative supersonic base pressure-coefficient levels roughly comparable to the XB-70 flight results for two engines off. This point may be of interest in the model simulation of the effects of losing thrust from an engine during transonic climbout for future side-by-side propulsion packages on supersonic- or hypersonic-cruise aircraft.

SUMMARY OF RESULTS

Comparison of full-scale flight pressure coefficients obtained from the base of the XB-70 propulsion package with predicted values provided the following results:

At cruise Mach numbers negative base pressure coefficients were expected on the basis of results from a wind-tunnel model with a flattened afterbody, boattail, and cold-air jet flow, and adjustments for the effects of temperature, partial shroud, and bleed flow. The full-scale propulsion package, however, experienced positive pressure coefficients at cruise Mach numbers. The increment of pressure coefficient separating the actual and predicted values at a Mach number of 2.8 was about 0.06, which represents a favorable increment of about 2 percent when interpreted in terms of lift-drag ratio.

At low supersonic speeds, predictions based on flight results from a two-engine side-by-side propulsion package underestimated the XB-70 flight values of negative base pressure coefficient, i.e., underestimated the base drag. At Mach numbers near 1.2,

the XB-70 flight values of negative base pressure coefficient were about three times larger than the predicted values.

The net calculated effect of underestimating the base drag at climbout speeds, even when overestimating the base drag at cruise, can seriously compromise the range potential of the aircraft, depending on several operational factors which can influence the transonic excess thrust. The trend of this range decrement with respect to the transonic excess thrust emphasizes the need for base pressure predictions based on models with a higher degree of similitude throughout the transonic and supersonic speed range.

The subsonic predictions based on wind-tunnel models with cold-air jet flow, adjusted for temperature effects, agreed with the flight results.

Flight Research Center,
National Aeronautics and Space Administration,
Edwards, Calif., December 1, 1967,
732-01-00-02-24.

REFERENCES

1. Love, Eugene S.: Base Pressure at Supersonic Speeds on Two-Dimensional Airfoils and on Bodies of Revolution With and Without Fins Having Turbulent Boundary Layers. NACA TN 3819, 1957. (Supersedes NACA RM L53C02.)

2. Chapman, Dean R.: An Analysis of Base Pressure at Supersonic Velocities and Comparison With Experiment. NACA Rept. 1051, 1951. (Supersedes NACA TN 2137.)

3. Chapman, Dean R.; Wimbrow, William R.; and Kester, Robert H.: Experimental Investigation of Base Pressure on Blunt-Trailing-Edge Wings at Supersonic Velocities. NACA Rept. 1109, 1952. (Supersedes NACA TN 2611.)

4. Chapman, Dean R.; Kuehn, Donald M.; and Larson, Howard K.: Investigation of Separated Flows in Supersonic and Subsonic Streams With Emphasis on the Effect of Transition. NACA Rept. 1356, 1958. (Supersedes NACA TN 3869.)

5. Korst, H. H.: A Theory for Base Pressures in Transonic and Supersonic Flow. J. Appl. Mech., vol. 23, no. 4, Dec. 1956, pp. 593-600.

6. Korst, H. H.; Chow, W. L.; and Zumwalt, G. W.: Research on Transonic and Supersonic Flow of a Real Fluid at Abrupt Increases in Cross Section (With Special Consideration of Base Drag Problems). ME Tech. Rep. 392-5, Univ. of Illinois, Dec. 1959.

7. Baughman, L. Eugene; and Kochendorfer, Fred D.: Jet Effects on Base Pressures of Conical Afterbodies at Mach 1.91 and 3.12. NACA RM E57E06, 1957.

8. Beheim, Milton A.: Flow in the Base Region of Axisymmetric and Two-Dimensional Configurations. NASA TR R-77, 1961.

9. Beheim, Milton A.; Klann, John L.; and Yeager, Richard A.: Jet Effects on Annular Base Pressure and Temperature in a Supersonic Stream. NASA TR R-125, 1962.

10. Nash, J. F.: A Discussion of Two-Dimensional Turbulent Base Flows. NPL Aero. Rep. 1162, National Physical Lab., British Aero. Res. Council, July 20, 1965.

11. Wolowicz, Chester H.; Strutz, Larry W.; Gilyard, Glenn B.; and Matheny, Neil W.: Preliminary Flight Evaluation of the Stability and Control Derivatives and Dynamic Characteristics of the Unaugmented XB-70-1 Airplane Including Comparisons With Predictions. NASA TN D-4578, 1968.

12. Saltzman, Edwin J.: Base Pressure Coefficients Obtained From the X-15 Airplane for Mach Numbers Up to 6. NASA TN D-2420, 1964.

13. Swihart, John M.; and Keith, Arvid L., Jr.: An Investigation of Clustered Jet-Exit Arrangements at Supersonic Speeds. NASA MEMO 5-11-59L, 1959.

14. Cubbage, James M., Jr.: Effect of Multiple-Jet Exits on the Base Pressure of a Simple Wing-Body Combination at Mach Numbers of 0.6 to 1.27. NASA TM X-25, 1959.

15. Raymes, Frederick: Multi-Jet Effects on Afterbody and Base Pressures at Supersonic Speeds (M = 2.5, 2.97, 3.46). Rep. No. NA58-1040, North American Aviation, Inc., Sept. 1958.

16. Swihart, John M.; and Nelson, William J.: Performance of Multiple Jet-Exit Installations. NACA RM L58E01, 1958.

17. Norton, Harry T., Jr.; Foss, Williard E., Jr.; and Swihart, John M.: An Investigation of Modified Clustered Jet-Exit Arrangements at Supersonic Speeds. NASA TM X-540, 1961.

18. B-70 Aerodynamic Project Group: Estimated Performance and Drag Substantiation Report for B-70 Primary Air Vehicle. Rep. No. NA-59-268, North American Aviation, Inc., Feb. 27, 1959. (Available from DDC as AD 331602L.)

19. B-70 Aerodynamic Project Group: Estimated Performance and Drag Substantiation Report for the B-70 Primary Air Vehicle. Rep. No. NA-59-268-1, North American Aviation, Inc., July 15, 1959. (Available from DDC as AD 331603L.)

20. Bowman, Paul V.: Estimated Performance Report for the XB-70A Air Vehicle No. 2. Rep. No. NA-65-661, North American Aviation, Inc., July 26, 1965.

21. Capone, Francis J.; Wornom, Dewey E.; and Igoe, William B.: Transonic Aerodynamic Characteristics of a Supersonic Canard-Airplane Model Modified for Use as a Recoverable Air-Breathing Booster. NASA TM X-698, 1962.

TABLE I. – GEOMETRIC CHARACTERISTICS OF THE XB-70-2 AIRPLANE

Total wing –		
Total area (includes 2482.34 ft^2 (230.62 m^2) covered by fuselage but not 33.53 ft^2 (3.12 m^2) of the wing ramp area), ft^2 (m^2)	6297.8	(585.07)
Span, ft (m)	105	(32)
Aspect ratio		1.751
Taper ratio		0.019
Dihedral angle, deg		5
Root chord (wing station 0), ft (m)	117.76	(35.89)
Tip chord (wing station 630 in. (16 m)), ft (m)	2.19	(0.67)
Mean aerodynamic chord (wing station 213.85 in. (5.43 m)), in. (m)	942.38	(23.94)
Fuselage station of 25-percent wing mean aerodynamic chord, in. (m)	1621.22	(41.18)
Sweepback angle, deg:		
Leading edge		65.57
25-percent element		58.79
Trailing edge		0
Incidence angle, deg:		
Root (fuselage juncture)		0
Tip (fold line and outboard)		-2.60
Airfoil section:		
Root to wing station 186 in. (4.72 m) (thickness-chord ratio, 2 percent)	0.30 to 0.70 HEX (MOD)	
Wing station 460 in. (11.68 m) to 630 in. (16 m) (thickness-chord ratio, 2.5 percent)	0.30 to 0.70 HEX (MOD)	
Inboard wing –		
Area (includes 2482.34 ft^2 (230.62 m^2) covered by fuselage but not 33.53 ft^2 (3.12 m^2) wing ramp area), ft^2 (m^2)	5256.0	(488.28)
Span, ft (m)	63.44	(19.34)
Aspect ratio		0.766
Taper ratio		0.407
Dihedral angle, deg		5
Root chord (wing station 0), ft (m)	117.76	(35.89)
Tip chord (wing station 380.62 in. (9.67 m)), ft (m)	47.94	(14.61)
Mean aerodynamic chord (wing station 163.58 in. (4.15 m)), in. (m)	1053	(26.75)
Fuselage station of 25-percent wing mean aerodynamic chord, in. (m)	1538.29	(39.07)
Sweepback angle, deg:		
Leading edge		65.57
25-percent element		58.79
Trailing edge		0
Airfoil section:		
Root (thickness-chord ratio, 2 percent)	0.30 to 0.70 HEX (MOD)	
Tip (thickness-chord ratio, 2.4 percent)	0.30 to 0.70 HEX (MOD)	

TABLE I. - GEOMETRIC CHARACTERISTICS OF THE XB-70-2 AIRPLANE - Continued

Mean camber (leading edge), deg:				
Butt plane 0				0.15
Butt plane 107 in. (2.72 m)				4.40
Butt plane 153 in. (3.89 m)				2.75
Butt plane 257 in. (6.53 m)				2.60
Butt plane 367 in. (9.32 m) to tip				0
Outboard wing -				
Area (one side only), ft^2 (m^2)			520.90	(48.39)
Span, ft (m)			20.78	(6.33)
Aspect ratio				0.829
Taper ratio				0.046
Dihedral angle, deg				5
Root chord (wing station 380.62 in. (9.67 m)), ft (m)			47.94	(14.61)
Tip chord (wing station 630 in. (16.00 m)), ft (m)			2.19	(0.67)
Mean aerodynamic chord (wing station 467.37 in. (11.87 m)), in. (m)			384.25	(9.76)
Sweepback angle, deg:				
Leading edge				65.57
25-percent element				58.79
Trailing edge				0
Airfoil section:				
Root (thickness-chord ratio, 2.4 percent)			0.30 to 0.70	HEX (MOD)
Tip (thickness-chord ratio, 2.5 percent)			0.30 to 0.70	HEX (MOD)
Down deflection from wing reference plane, deg				0, 30, 70
Skewline of tip fold, deg:				
Leading edge in				1.5
Leading edge down				3
Wing-tip area in wing reference plane (one side only), ft^2 (m^2):				
Rotated down 30°			472.04	(43.85)
Rotated down 70°			220.01	(20.44)
	Wing tips			
	Up		Down	
Elevons (data for one side):				
Total area aft of hinge line, ft^2 (m^2)	197.7	(18.37)	135.26	(12.57)
Span, ft (m)	20.44	(6.23)	13.98	(4.26)
Inboard chord (equivalent), in. (m)	116	(2.95)	116	(2.95)
Outboard chord (equivalent), in. (m)	116	(2.95)	116	(2.95)
Sweepback angle of hinge line, deg	0		0	
Deflection, deg:				
As elevator				-25 to 15
As aileron with elevators at ±15° or less				-15 to 15
As aileron with elevators at -25°				-5 to 5
Total				-30 to 30
Canard -				
Area (includes 150.31 ft^2 (13.96 m^2) covered by fuselage), ft^2 (m^2)			415.59	(38.61)
Span, ft (m)			28.81	(8.78)

TABLE I. – GEOMETRIC CHARACTERISTICS OF THE XB-70-2 AIRPLANE - Continued

Aspect ratio	1.997	
Taper ratio	0.388	
Dihedral angle, deg	0	
Root chord (canard station 0), ft (m)	20.79	(6.34)
Tip chord (canard station 172.86 in. (4.39 m)), ft (m)	8.06	(2.46)
Mean aerodynamic chord (canard station 73.71 in. (1.87 m)), in. (m)	184.3	(4.68)
Fuselage station of 25-percent canard mean aerodynamic chord, in. (m)	553.73	(14.06)
Sweepback angle, deg:		
Leading edge	31.70	
25-percent element	21.64	
Trailing edge	-14.91	
Incidence angle (nose up), deg	0 to 6	
Airfoil section:		
Root (thickness-chord ratio 2.5 percent)	0.34 to 0.66 HEX (MOD)	
Tip (thickness-chord ratio 2.52 percent)	0.34 to 0.66 HEX (MOD)	
Ratio of canard area to wing area	0.066	
Canard flap (one of two):		
Area (aft of hinge line), ft^2 (m^2)	54.69	(5.08)
Ratio of flap area to canard semi-area	0.263	
Vertical tail (one of two) –		
Area (includes 8.96 ft^2 (0.83 m^2) blanketed area), ft^2 (m^2)	233.96	(21.74)
Span, ft (m)	15	(4.57)
Aspect ratio	1	
Taper ratio	0.30	
Root chord (vertical-tail station 0), ft (m)	23.08	(7.03)
Tip chord (vertical-tail station 180 in. (4.57 m)), ft (m)	6.92	(2.11)
Mean aerodynamic chord (vertical-tail station 73.85 in. (1.88 m)), in. (m)	197.40	(5.01)
Fuselage station of 25-percent vertical-tail mean aerodynamic chord, in. (m)	2188.50	(55.59)
Sweepback angle, deg:		
Leading edge	51.77	
25-percent element	45	
Trailing edge	10.89	
Airfoil section:		
Root (thickness-chord ratio 3.75 percent)	0.30 to 0.70 HEX (MOD)	
Tip (thickness-chord ratio 2.5 percent)	0.30 to 0.70 HEX (MOD)	
Cant angle, deg	0	
Ratio vertical tail to wing area	0.037	
Rudder travel, deg:		
With gear extended	±12	
With gear retracted	±3	
Fuselage (includes canopy) –		
Length, ft (m)	185.75	(56.62)
Maximum depth (fuselage station 878 in. (22.30 m)), in. (m)	106.92	(2.72)

TABLE I – GEOMETRIC CHARACTERISTICS OF THE XB-70-2 AIRPLANE - Concluded

Maximum breadth (fuselage station 855 in. (21.72 m)), in. (m)	100	(2.54)
Side area, ft^2 (m^2)	939.72	(87.30)
Planform area, ft^2 (m^2)	1184.78	(110.07)
Center of gravity:		
Forward limit, percent mean aerodynamic chord		19.0
Aft limit, percent mean aerodynamic chord		25.0
Duct –		
Length, ft (m)	104.84	(31.96)
Maximum depth (fuselage station 1375 in. (34.93 m)), in. (m)	90.75	(2.31)
Maximum breadth (fuselage station 2100 in. (53.34 m)), in. (m)	360.70	(9.16)
Side area, ft^2 (m^2)	716.66	(66.58)
Planform area, ft^2 (m^2)	2342.33	(217.61)
Inlet captive area (each), $in.^2$ (m^2)	5600	(3.61)
Surface areas (net wetted), ft^2 (m^2) –		
Fuselage and canopy	2871.24	(266.75)
Duct	4956.66	(460.49)
Wing, wing tips, and wing ramp	7658.44	(711.49)
Vertical tails (two)	936.64	(87.02)
Canard	530.83	(49.32)
Tail pipes	340.45	(31.62)
Total	17,294.26	(1606.69)
Engines	6 YJ93-GE-3	

TABLE II. – PHYSICAL CHARACTERISTICS OF XB-70 BASE AND ENGINE

Boattail angle, deg –		
Upper surface		6
Lower surface		5
Side		6
Base areas, ft^2 (m^2) –		
Total	137	(12.7)
Total (all engines on, minimum exit area)	107.2	(10)
Total (all engines on, maximum exit area)	48.5	(4.5)
Projected thickness (height) of base, in. (m)	58	(1.47)
Width of propulsion package, in. (cm)	360	(914)
Linear dimension pertinent to orifices, in. (cm) –		
Orifices 1, 3, 4, 6, 7, 8, 9, 10, 11	63.5	(161)
Orifices 2 and 5	11.5	(29)
Engine –		
Jet-exit area (minimum), $in.^2$ (cm^2)	715	(4613)
Jet-exit area (maximum), $in.^2$ (cm^2)	2120	(13,678)
Jet-exit diameter (minimum), in. (cm)	30.2	(77)
Jet-exit diameter (maximum), in. (cm)	52	(132)

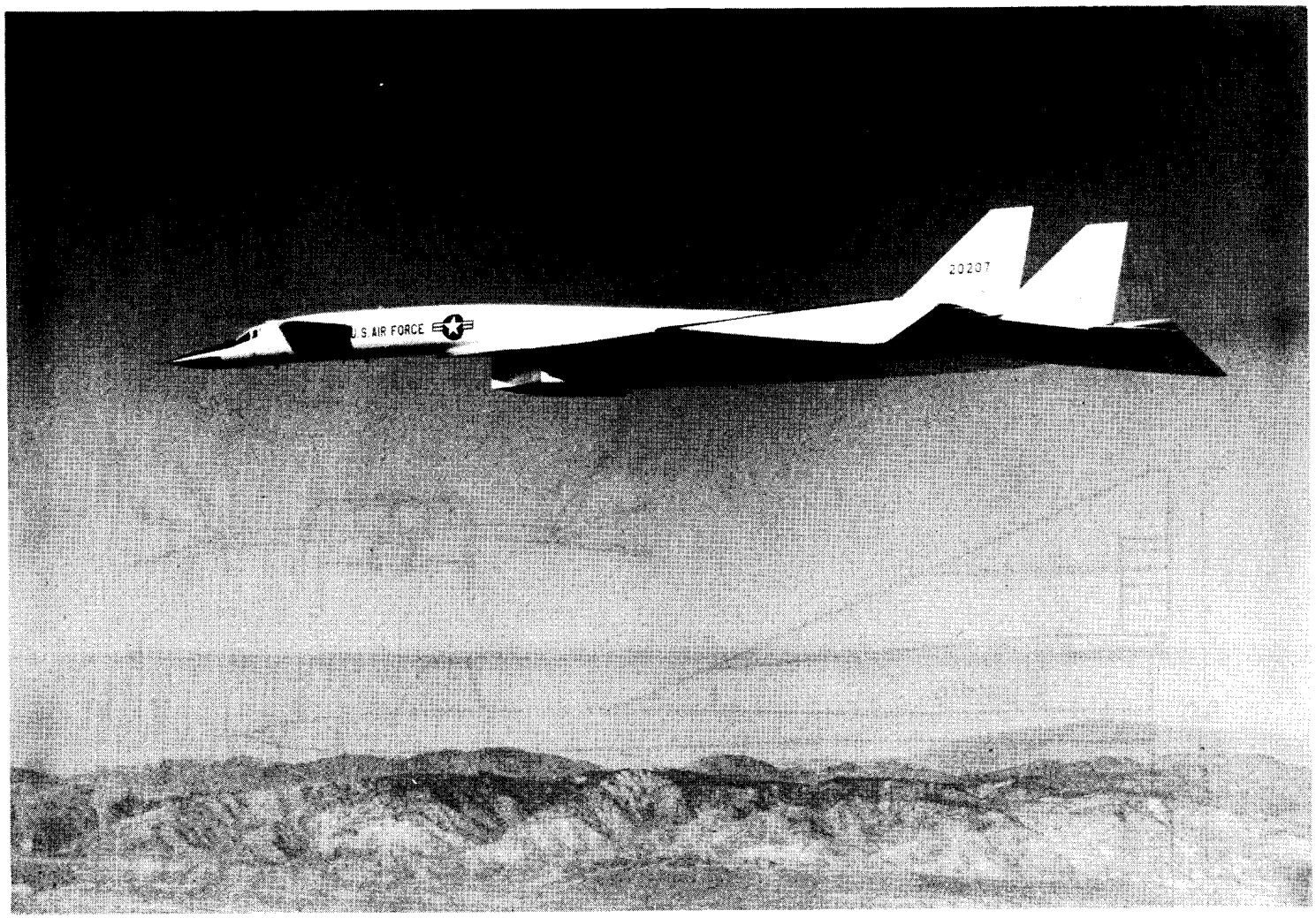

Figure 1. – XB-70 airplane.

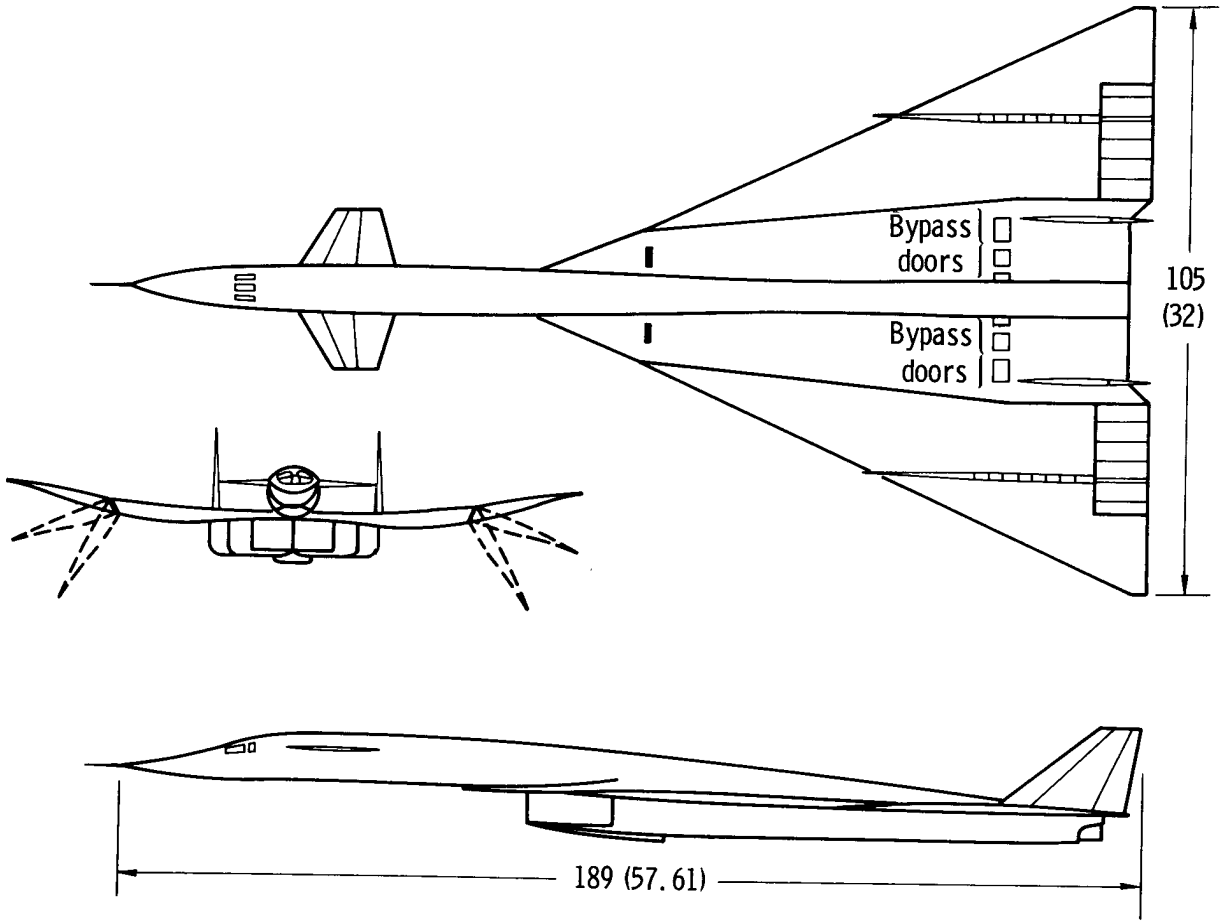

Figure 2.– Three-view drawing of the XB-70 airplane. Dimensions in feet (meters).

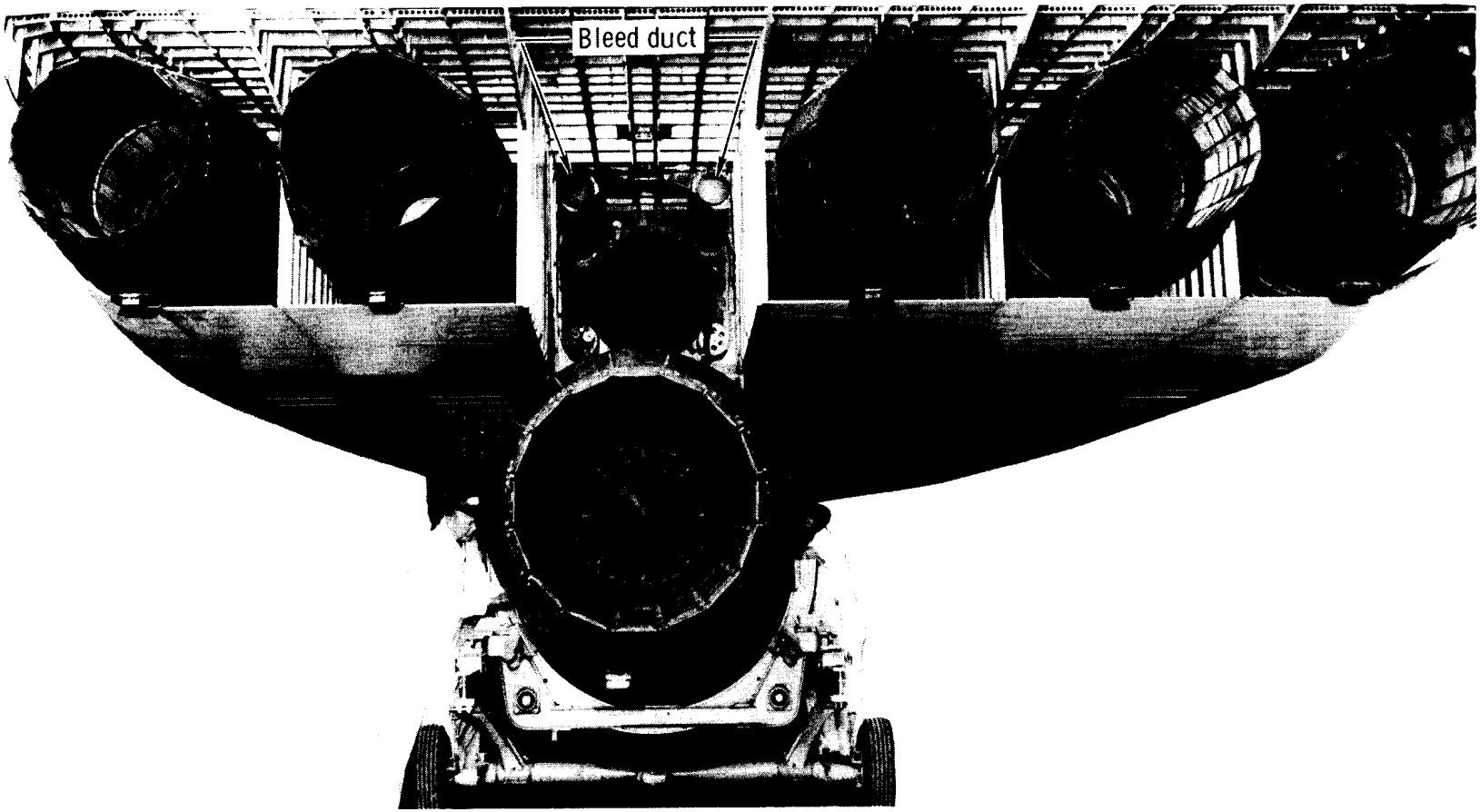

Figure 3. – Rear view of the XB-70 airplane with engine 3 removed.
(Non-pertinent items have been deleted.)

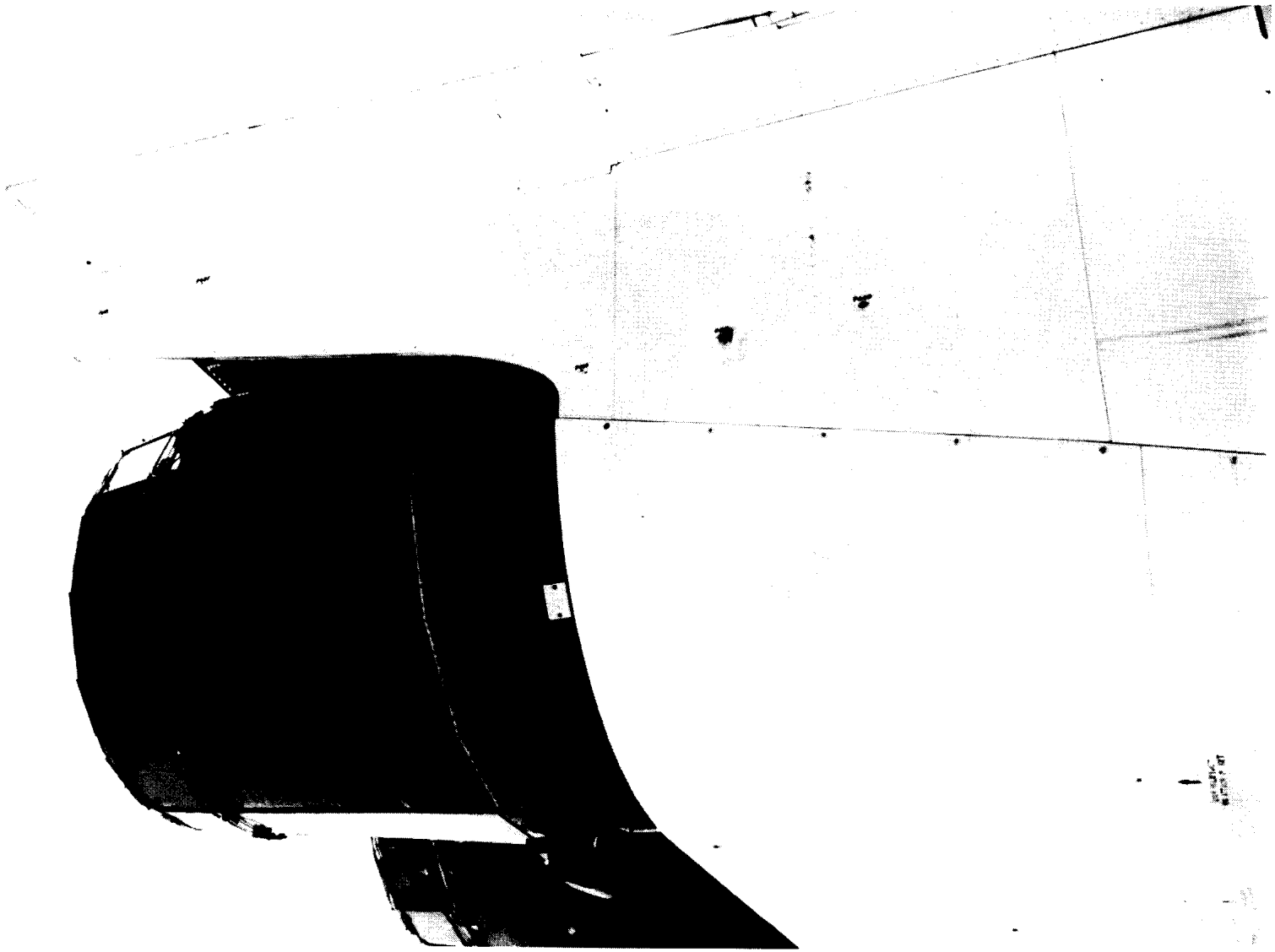

Figure 4.– XB-70 viewed from right rear illustrating overhang of the engine nozzles beyond the lower boattail.

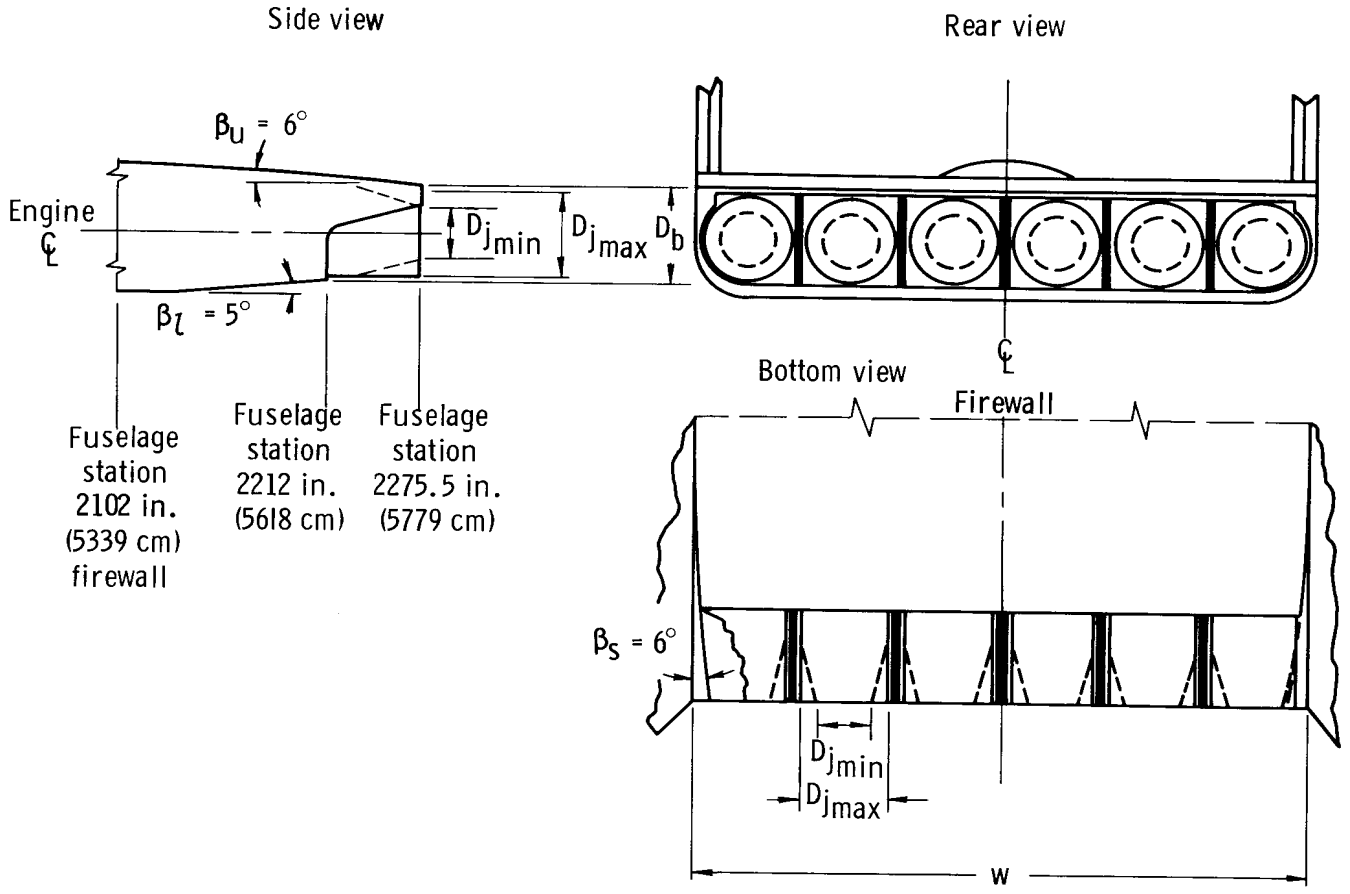

Figure 5.– Three-view drawing of XB-70 afterbody showing pertinent dimensions $D_{j_{max}}$ = 52 in. (132 cm); $D_{j_{min}}$ = 30.2 in. (77 cm); D_b = 58 in. (147 cm); w = 360 in. (914 cm).

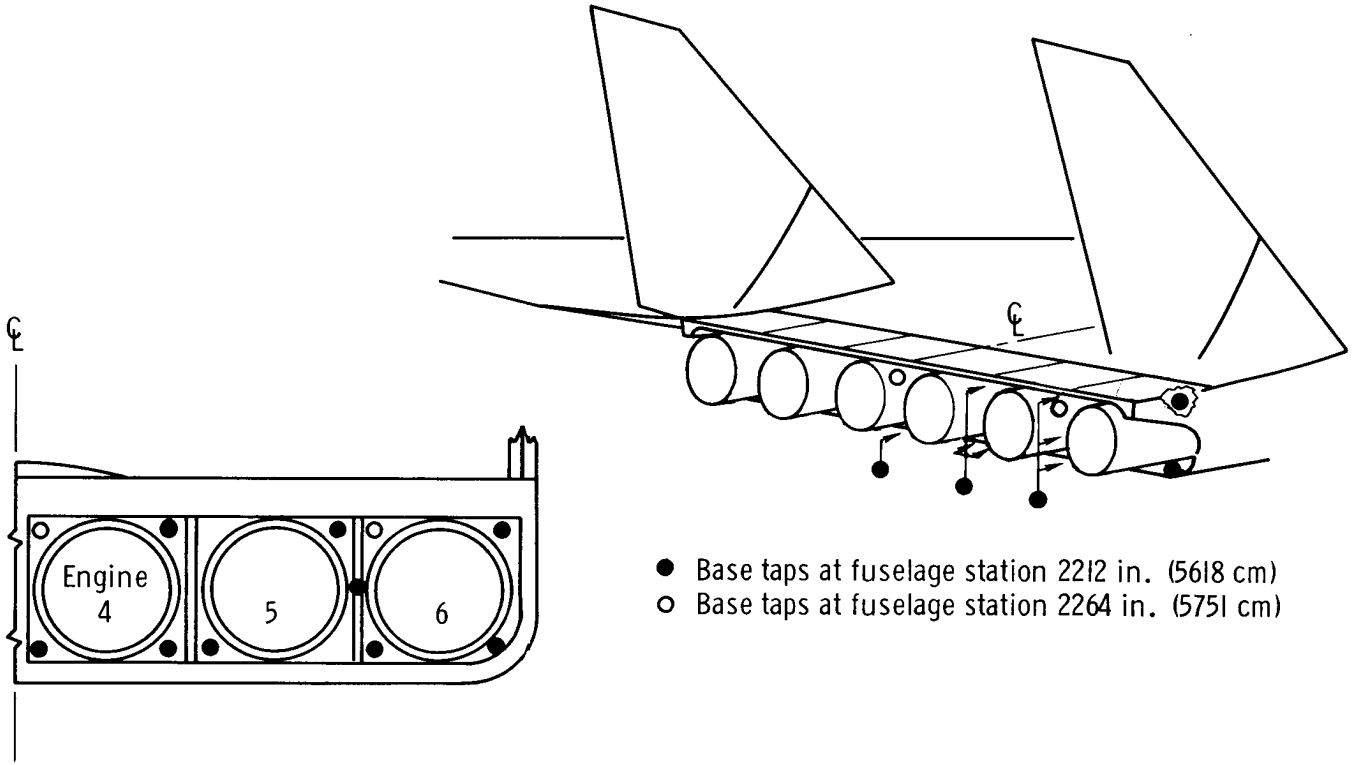

Figure 6. – Schematic drawing of XB-70 base showing location of base pressure static orifices.

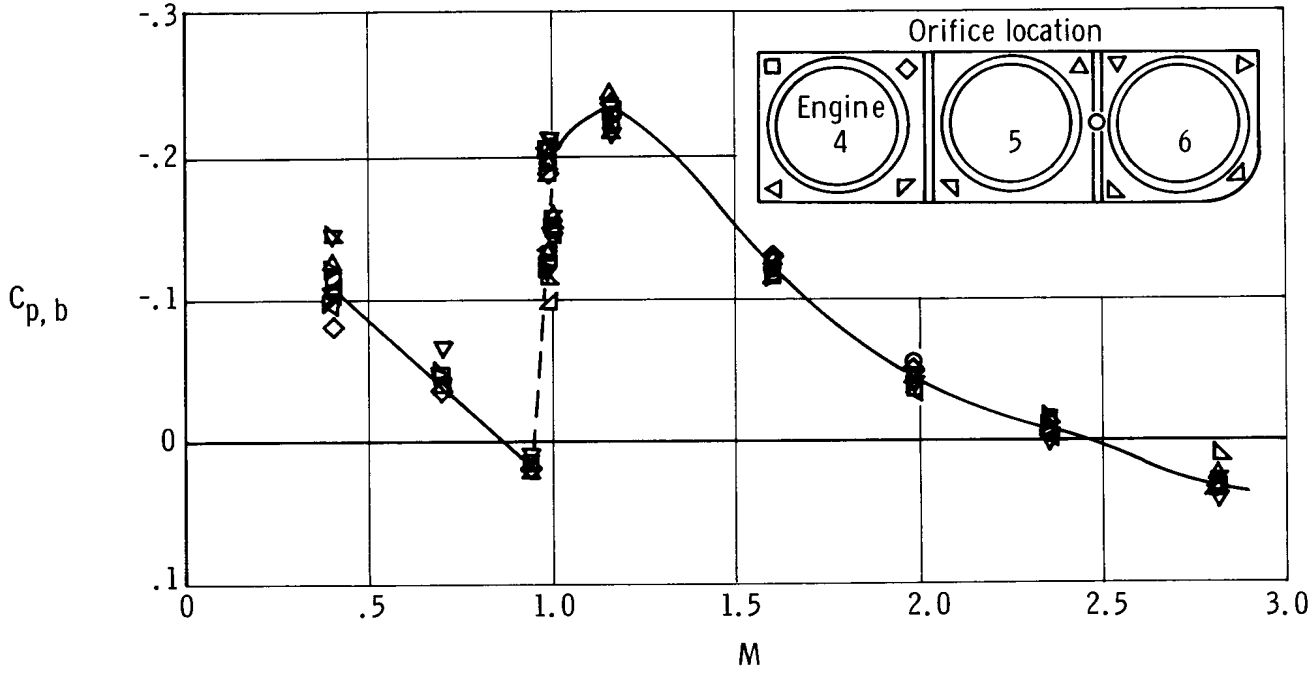

Figure 7.– Variation of base pressure coefficient with Mach number for the individual orifices. All engines operating at afterburner power setting.

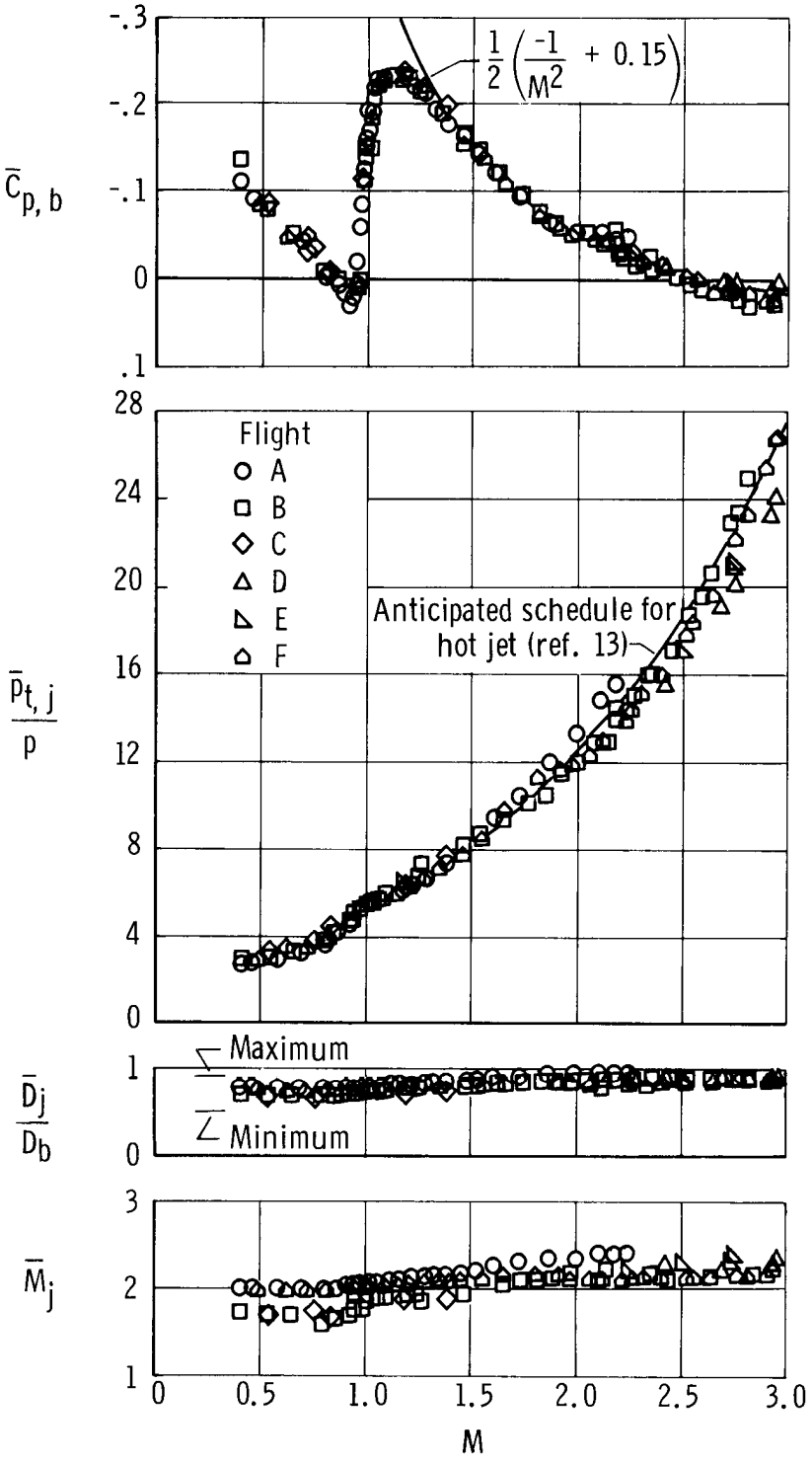

Figure 8. – Average base pressure coefficient and primary parameters affecting base pressure as a function of free-stream Mach number. All engines operating at afterburner power setting; turbulent flow; $\frac{N_{Re}}{l} = 1.05 \times 10^6$ to 3.72×10^6 per foot (3.44×10^6 to 12.20×10^6 per meter); $\alpha = 2.1°$ to $9.5°$.

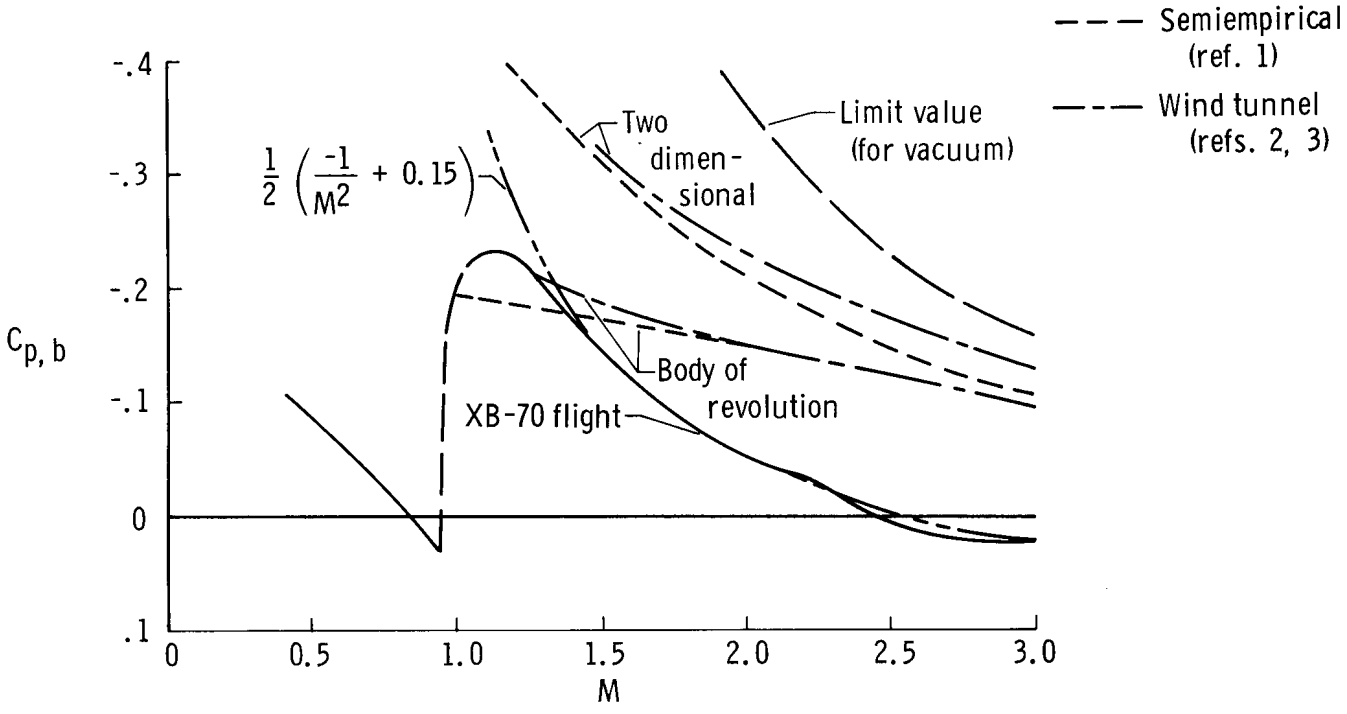

Figure 9.– Comparison of flight-measured XB-70 average base pressure coefficient with wind-tunnel results and semiempirical estimates for two- and three-dimensional shapes. No jet flow for models or semiempirical estimates.

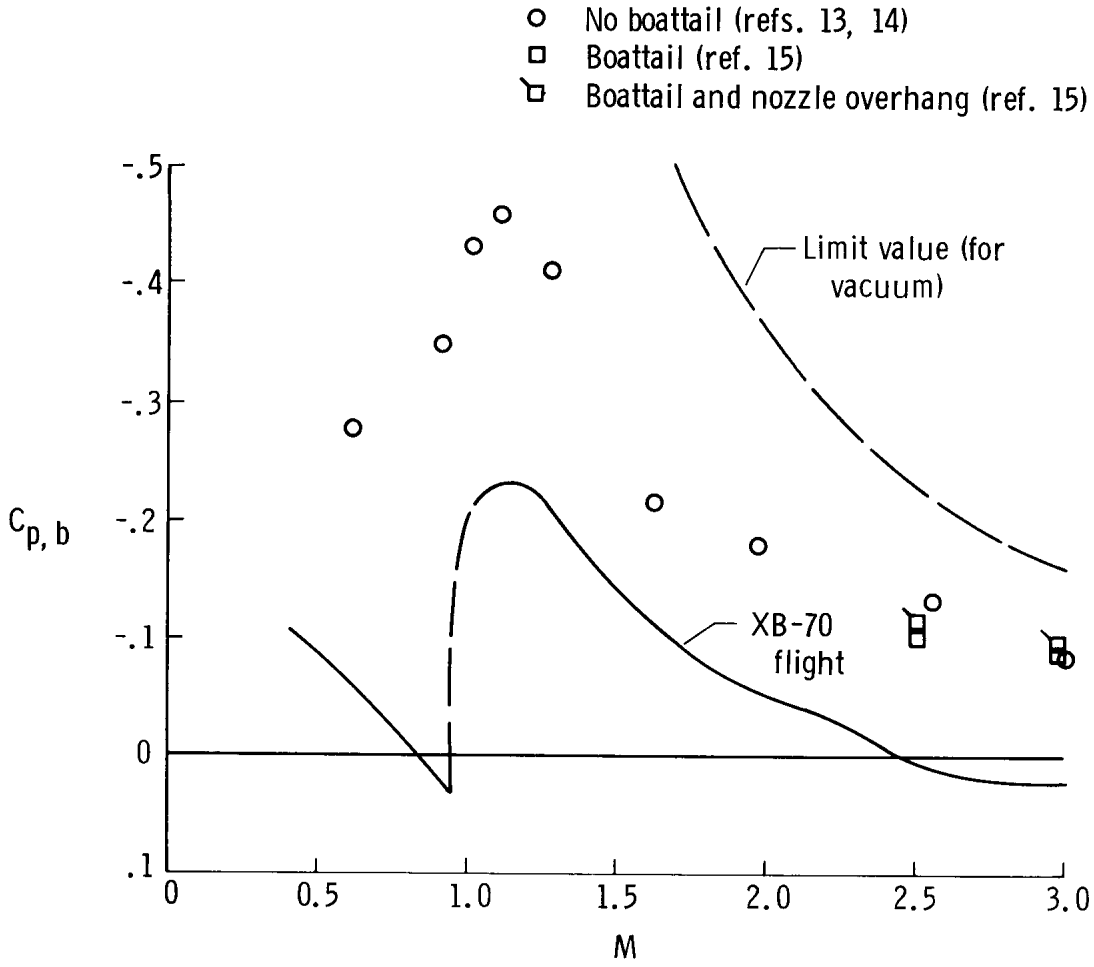

Figure 10.– Comparison of flight-measured XB-70 average base pressure coefficient with models having flattened afterbodies. No jet flow for models.

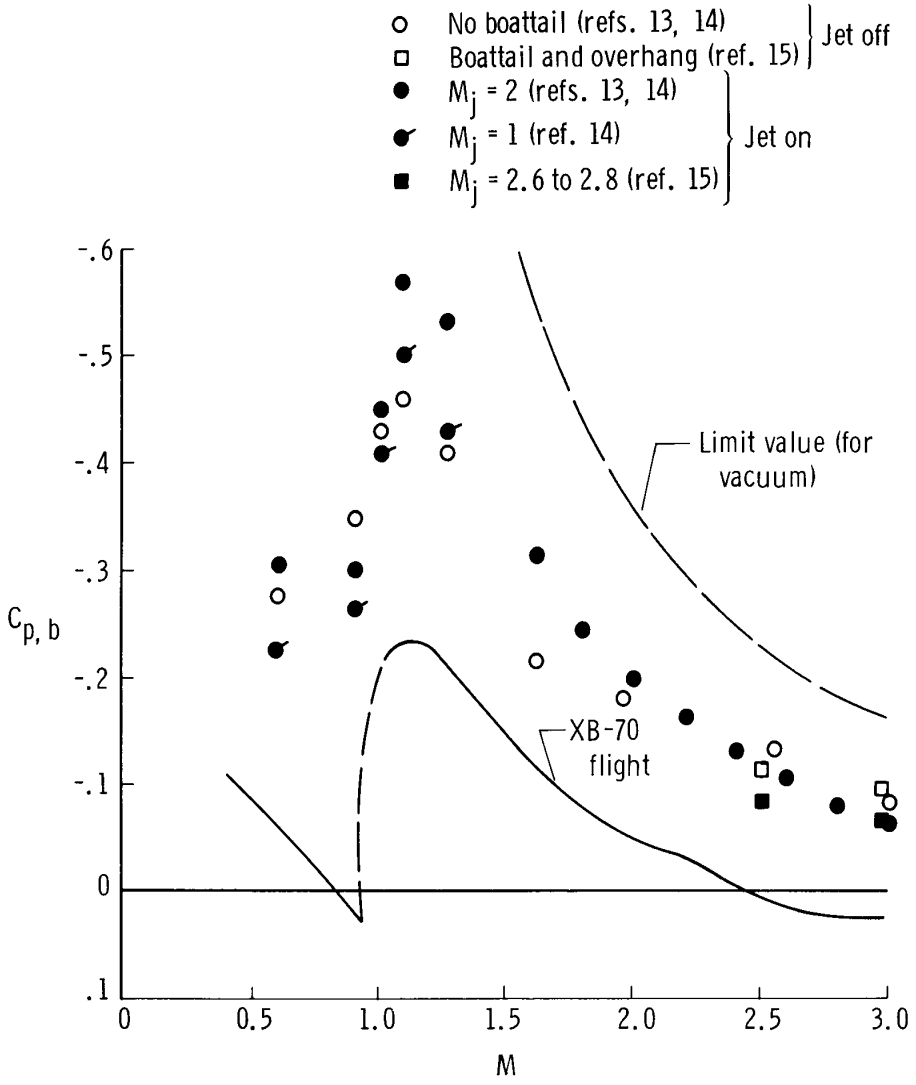

Figure 11.– Comparison of flight-measured XB-70 average base pressure coefficient with models having flattened afterbodies, including cold-air jet flow.

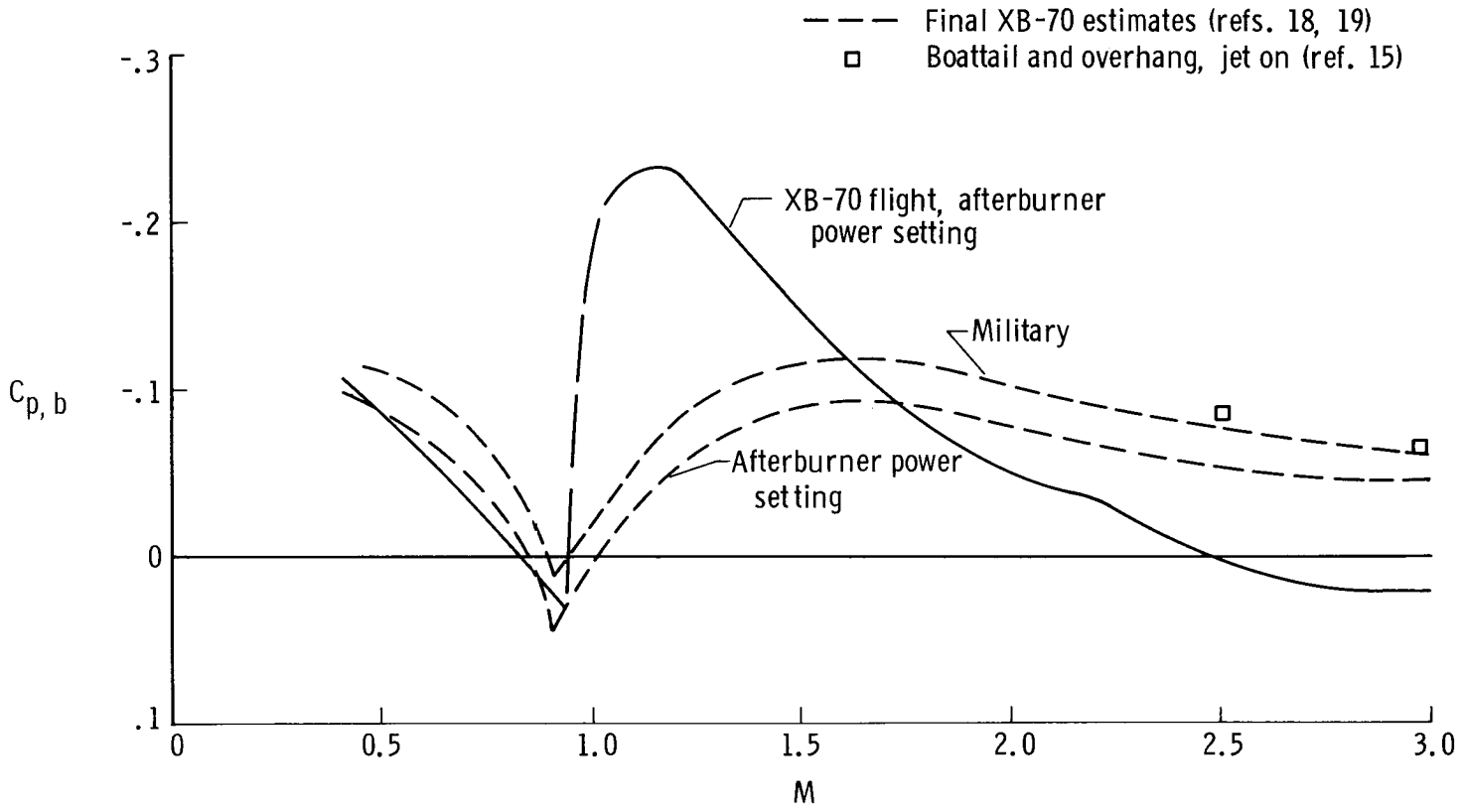

Figure 12.– Comparison of flight-measured XB-70 average base pressure coefficient with predicted values.

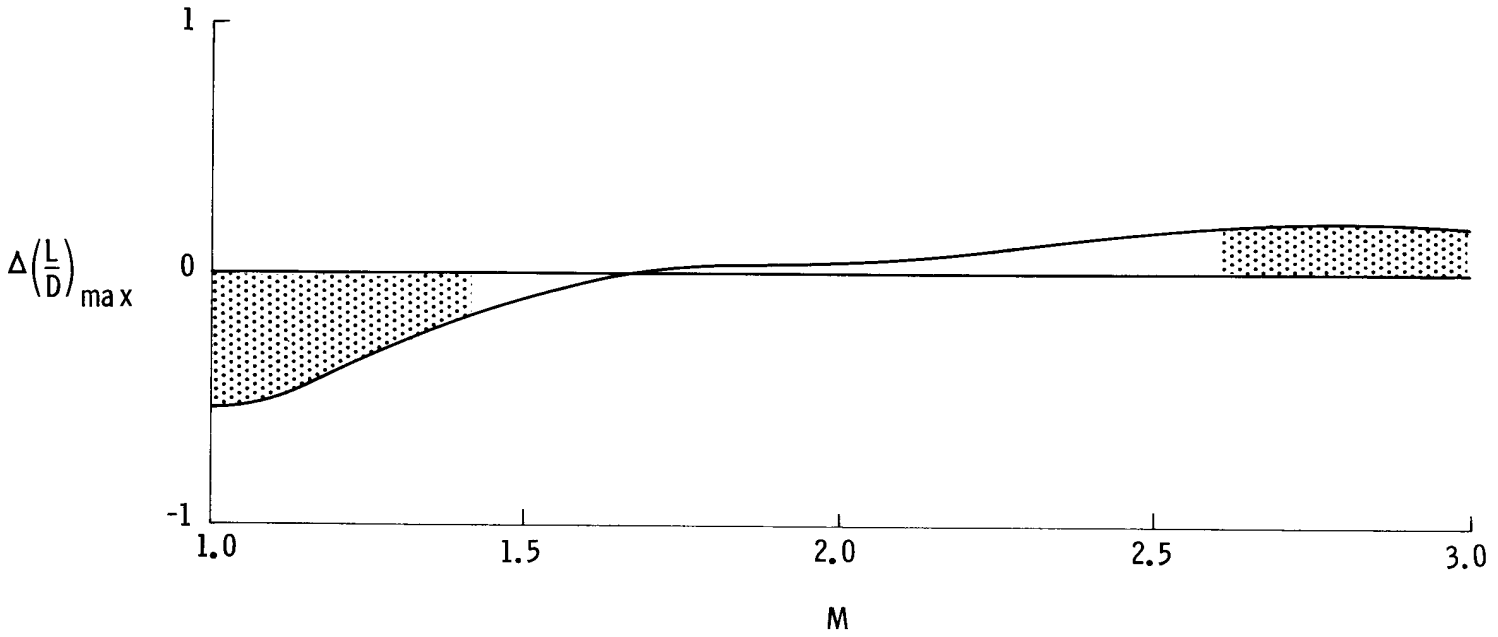

Figure 13. – Calculated increment of $\frac{L}{D}$ resulting from difference between predicted and measured base pressure coefficients. (Only $\Delta\frac{L}{D}$ in shaded regions used for range-increment calculations.)

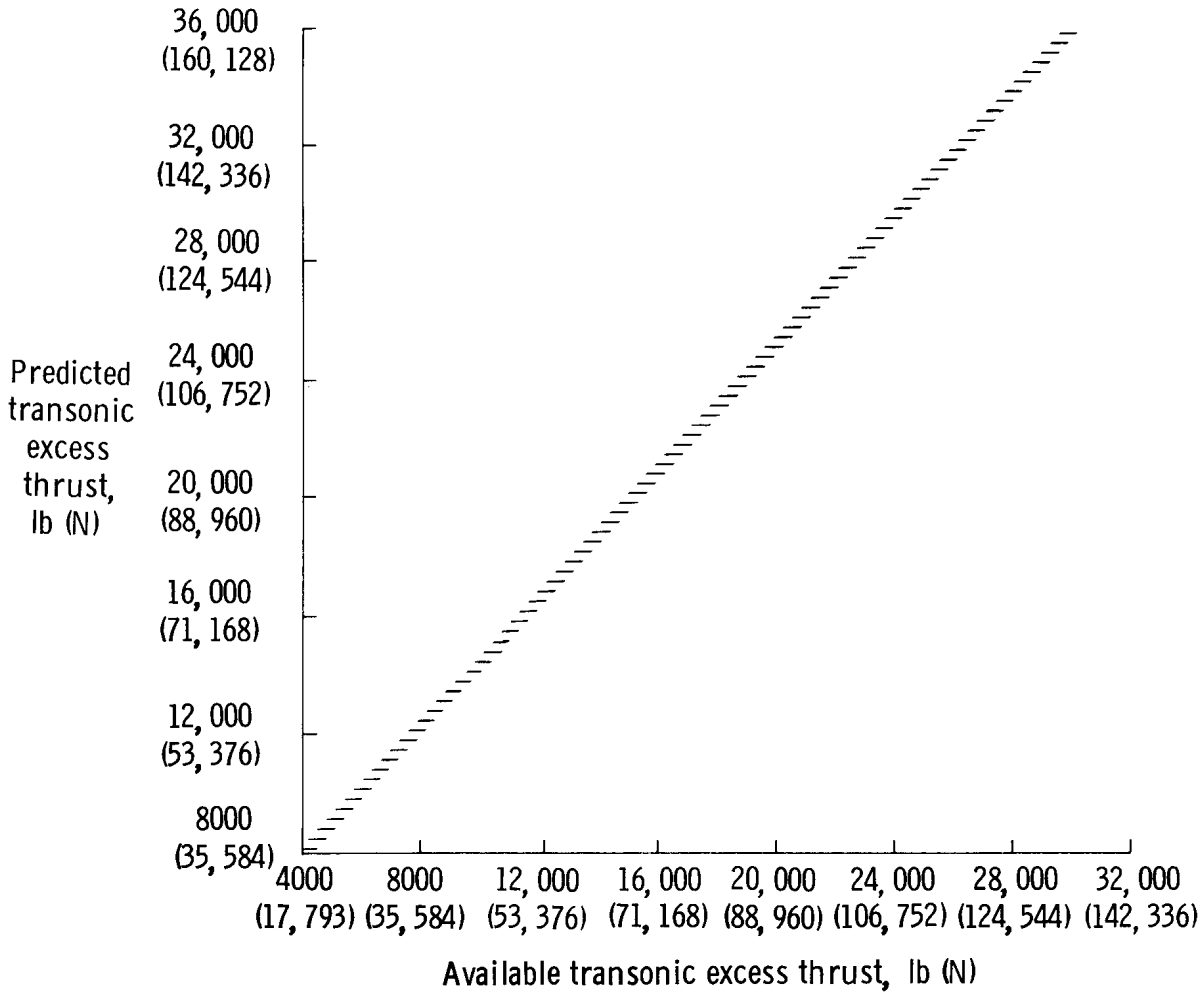

(a) Relationship of the available transonic excess thrust to the predicted transonic excess thrust. M = 1.0 to 1.4.

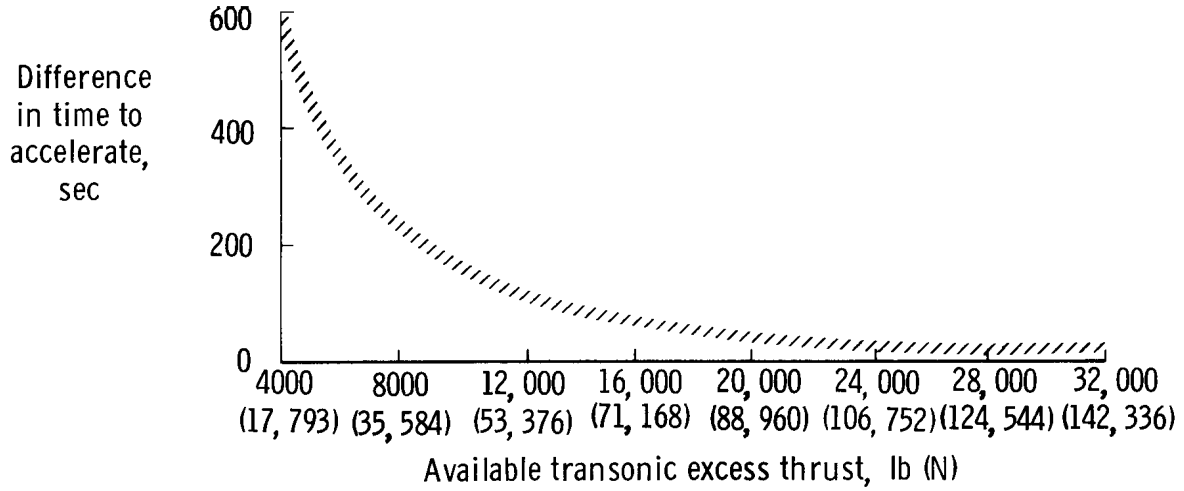

(b) Estimated difference in time to accelerate caused by mispredicting base pressure. M = 1.0 to 1.4.

Figure 14. – Effects of mispredicting base pressure on several performance parameters. Mean transonic weight = 425,000 lb (192,700 kg).

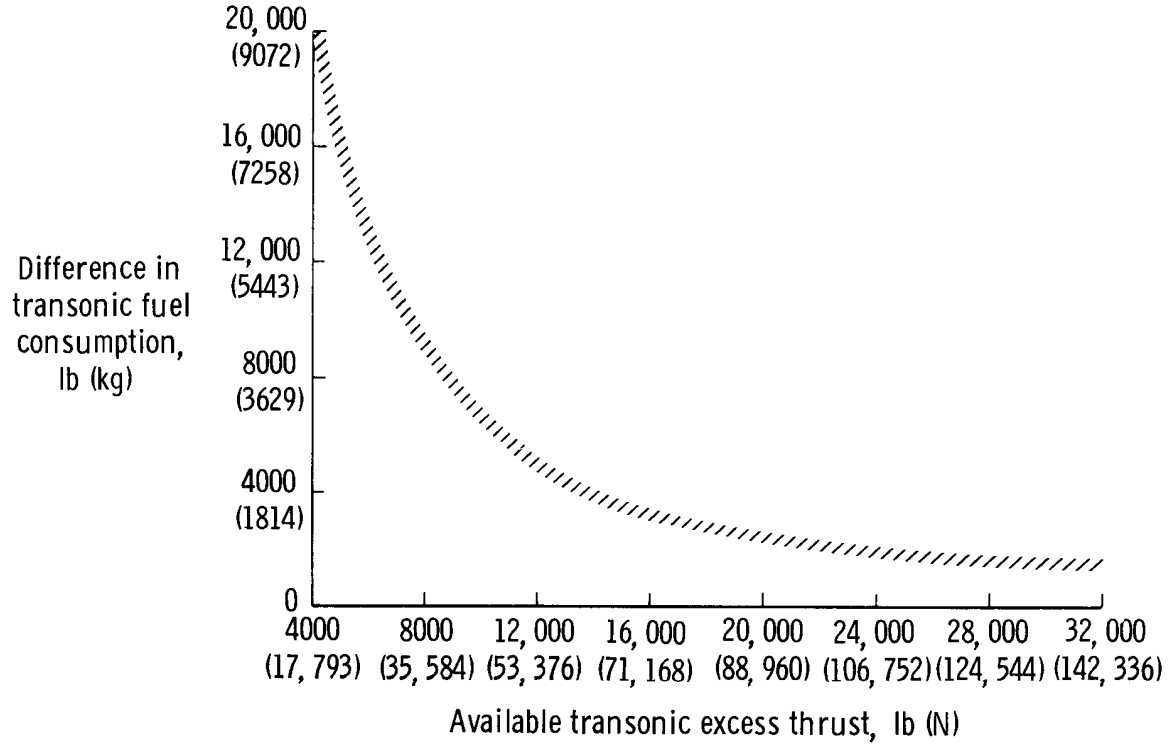

(c) Estimated difference in transonic fuel consumption caused by mispredicting base pressure. M = 1.0 to 1.4.

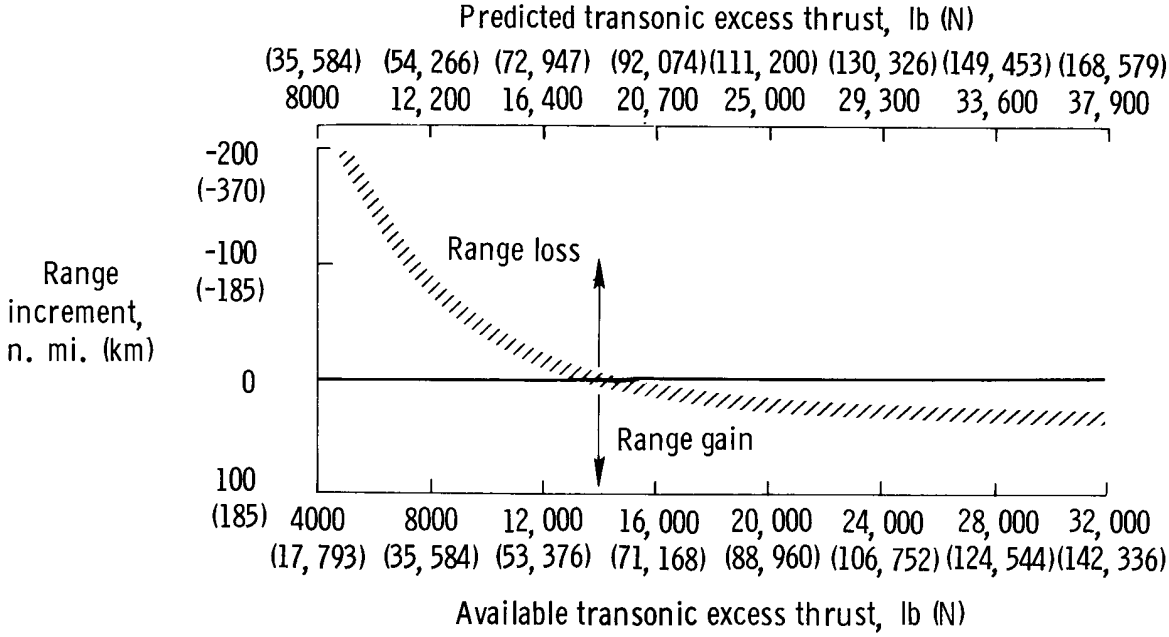

(d) Estimated gross range variation caused by mispredicting base pressure as a function of predicted and available transonic excess thrust.

Figure 14. – Concluded.

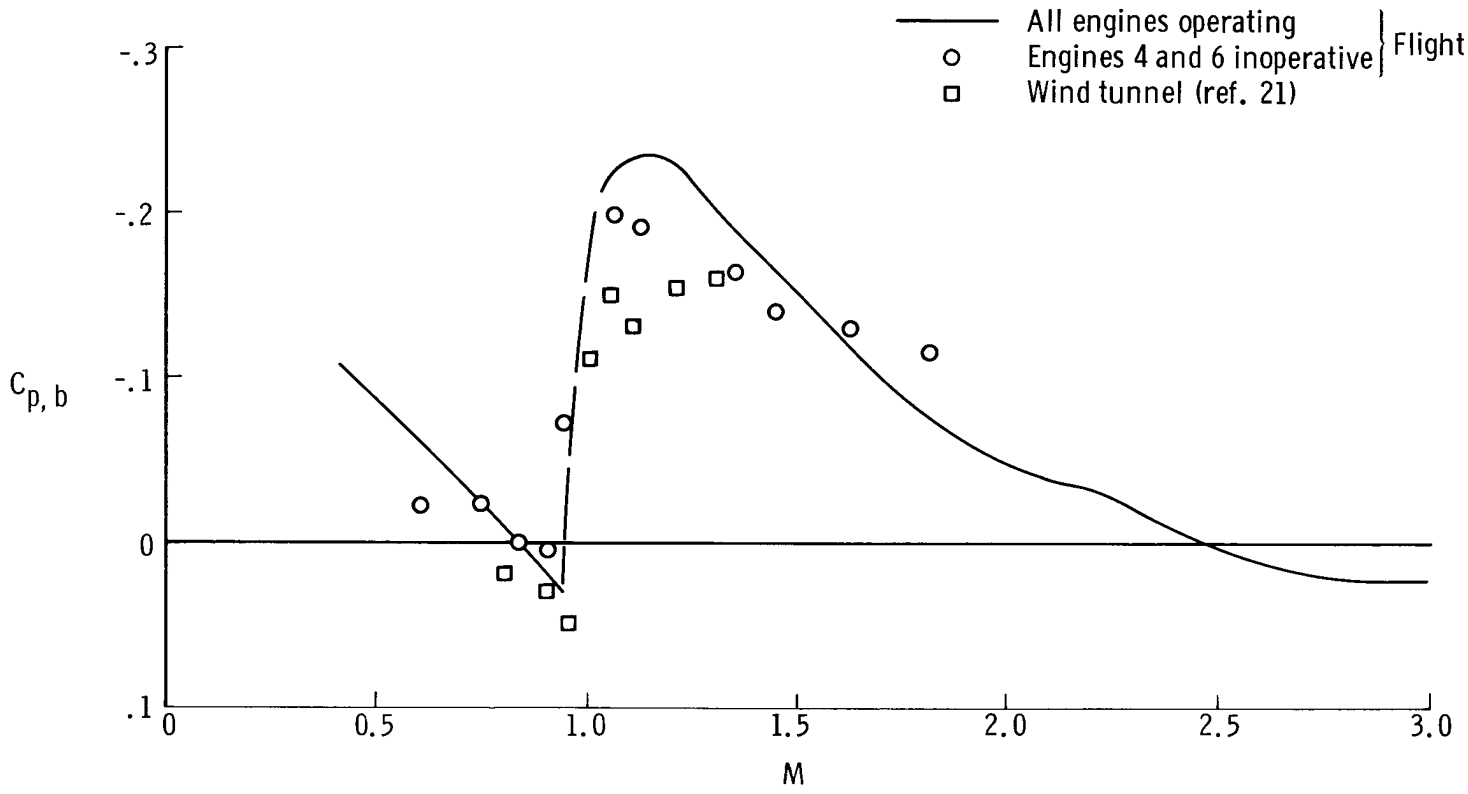

Figure 15.– Comparison of flight-measured average base pressure coefficient for the XB-70 with vented-base wind-tunnel-model results.